The current issue and full text archive of this journal is available at
www.emeraldinsight.com/1573-6105.htm

Received 3 January 2014
Revised 1 March 2014
Accepted 19 April 2014

Analysis of steel-with-composite material substitution in military vehicle hull floors subjected to shallow-buried landmine-detonation loads

M. Grujicic, J.S. Snipes, S. Ramaswami and R. Yavari
Department of Mechanical Engineering, Clemson University, Clemson, South Carolina, USA, and
C.-F. Yen and B.A. Cheeseman
Army Research Laboratory – Weapons & Materials Research Directorate, Proving Ground, Maryland, USA

Abstract

Purpose – The purpose of this paper is to address the problem of substitution of steel with fiber-reinforced polymer-matrix composite in military-vehicle hull-floors, and identifies and quantifies the associated main benefits and shortcomings.

Design/methodology/approach – The problem is investigated using a combined finite-element/discrete-particle computational analysis. Within this analysis, soil (in which a landmine is buried), gaseous detonation products and air are modeled as assemblies of discrete, interacting particles while the hull-floor is treated as a Lagrangian-type continuum structure. Considerable effort has been invested in deriving the discrete-material properties from the available experimental data. Special attention has been given to the derivation of the contact properties since these, in the cases involving discrete particles, contain a majority of the information pertaining to the constitutive response of the associated materials. The potential ramifications associated with the aforementioned material substitution are investigated under a large number of mine-detonation scenarios involving physically realistic ranges of the landmine mass, its depth of burial in the soil, and the soil-surface/floor-plate distances.

Findings – The results obtained clearly revealed both the benefits and the shortcomings associated with the examined material substitution, suggesting that they should be properly weighted in each specific case of hull-floor design.

Originality/value – To the authors' knowledge, the present work is the first public-domain report of the findings concerning the complexity of steel substitution with composite-material in military-vehicle hull-floors.

Keywords Blast and soil ejecta loading, Detonation of shallow buried mines, Discrete-particle approach

Paper type Research paper

The material presented in this paper is based on work supported by three Army Research Office sponsored grants entitled "Multi-length Scale Material Model Development for Armor-grade Composites" (Contract No. W911NF-09-1-0513), "Friction Stir Welding Behavior of Selected 2000-series and 5000-series Aluminum Alloys" (Contract No. W911NF-11-1-0207), and "Concept Validation and Optimization for a Vent-based Mine-blast Mitigation System" (Contract No. W911NF-11-1-0518).

Multidiscipline Modeling in Materials and Structures
Vol. 10 No. 3, 2014
pp. 416-448

1573-6105
DOI 10.1108/MMMS-01-2014-0001

Report Documentation Page

Form Approved
OMB No. 0704-0188

1. REPORT DATE	2. REPORT TYPE	3. DATES COVERED
2014		**00-00-2014 to 00-00-2014**

4. TITLE AND SUBTITLE
Analysis of Steel-with-composite Material Substitution in Military Vehicle Hull Floors Subjected to Shallow-buried Landmine-detonation Loads

5a. CONTRACT NUMBER
5b. GRANT NUMBER
5c. PROGRAM ELEMENT NUMBER

6. AUTHOR(S)

5d. PROJECT NUMBER
5e. TASK NUMBER
5f. WORK UNIT NUMBER

7. PERFORMING ORGANIZATION NAME(S) AND ADDRESS(ES)
Clemson University,Department of Mechanical Engineering,241 Engineering Innovation Building,Clemson,SC,29634

8. PERFORMING ORGANIZATION REPORT NUMBER

9. SPONSORING/MONITORING AGENCY NAME(S) AND ADDRESS(ES)

10. SPONSOR/MONITOR'S ACRONYM(S)
11. SPONSOR/MONITOR'S REPORT NUMBER(S)

12. DISTRIBUTION/AVAILABILITY STATEMENT
Approved for public release; distribution unlimited

13. SUPPLEMENTARY NOTES

14. ABSTRACT

Purpose ??? The purpose of this paper is to address the problem of substitution of steel with fiberreinforced polymer-matrix composite in military-vehicle hull-floors, and identifies and quantifies the associated main benefits and shortcomings. Design/methodology/approach ??? The problem is investigated using a combined finite-element/ discrete-particle computational analysis. Within this analysis, soil (in which a landmine is buried) gaseous detonation products and air are modeled as assemblies of discrete, interacting particles while the hull-floor is treated as a Lagrangian-type continuum structure. Considerable effort has been invested in deriving the discrete-material properties from the available experimental data. Special attention has been given to the derivation of the contact properties since these, in the cases involving discrete particles, contain a majority of the information pertaining to the constitutive response of the associated materials. The potential ramifications associated with the aforementioned material substitution are investigated under a large number of mine-detonation scenarios involving physically realistic ranges of the landmine mass, its depth of burial in the soil, and the soil-surface/floor-plate distances. Findings ??? The results obtained clearly revealed both the benefits and the shortcomings associated with the examined material substitution, suggesting that they should be properly weighted in each specific case of hull-floor design. Originality/value ??? To the authors??? knowledge, the present work is the first public-domain report of the findings concerning the complexity of steel substitution with composite-material in military-vehicle hull-floors.

15. SUBJECT TERMS

16. SECURITY CLASSIFICATION OF:			17. LIMITATION OF ABSTRACT	18. NUMBER OF PAGES	19a. NAME OF RESPONSIBLE PERSON
a. REPORT	b. ABSTRACT	c. THIS PAGE			
unclassified	**unclassified**	**unclassified**	**Same as Report (SAR)**	**33**	

1. Introduction

In the present work, the kinematic and structural (including failure/fracture) response of a military-vehicle hull-floor (either made of steel or light-weighted through the use of high-performance polymer-matrix composites) subjected to blast loads resulting from the detonation of shallow-buried land-mines has been investigated using a combined finite-element/discrete-particle computational analysis. Hence, the main topics to be overviewed in this introductory section of the present manuscript include: the need for light-weight military vehicles; the role of the military-vehicle hull-floor; detonation of shallow-buried mines; landmine-detonation-induced impulse loading; and use of computer-aided engineering. As far as a review of the computational methods used in the analysis of various mine-blast scenarios is concerned, it will be presented in Section 2.

1.1 The need for light-weight military vehicles

Recent efforts of the US Army have been aimed at becoming more mobile, deployable, and sustainable while maintaining or surpassing the current levels of lethality and survivability. Current battlefield vehicles have reached in excess of 70 tons due to ever increasing lethality of ballistic threats which hinders their ability to be readily transported and sustained. Therefore, a number of research and development programs are under way to engineer light-weight, highly mobile, transportable and lethal battlefield vehicles with a target weight under 20 tons. To attain these goals, significant advances are needed in the area of light-weight materials and structures as well as in the area of computer-aided design and experimental testing/validation techniques for these vehicles. Advances in both of these areas are addressed in the present work.

1.2 The role of the military-vehicle hull-floor

The main role of the military-vehicle hull-floor is to protect the vehicle occupants in the case of detonation of a landmine buried in soil underneath the vehicle belly. Complex interrelationships generally exist between the type and the extent of vehicle-occupants' injuries, and the extent of vehicle damage resulting from under-the-vehicle landmine blast. The most serious vehicle-occupant injuries and their fatalities are most frequently incurred as a consequence of hull-floor rupture. In addition to generating floor-material fragmentation, floor rupture enables the ingress of flame and toxic (detonation-product) gases and can lead to on-board fires and explosions. While the vehicle under landmine attack is always subjected to high gravitational forces, this aspect of the threat is usually considered as secondary when floor rupture takes place. On the other hand, when landmine detonation results in only hull-floor bulging, the vehicle is then propelled upward and off the ground, to an extent which scales directly with size of the landmine and inversely with vehicle weight. The accompanying dynamic shock can cause vehicle occupants and on-board instruments and weapons to be thrown about within the vehicle interior. In addition, large hull-floor deflections and deformations, as well as a large number of fragments spalled off from the top face of the floor, can cause a sequence of failures throughout the entire vehicle through components/sub-system connections and interfaces (e.g. via fuel lines running along the floor, floor-bolted seats, ammunition storage racks, power-train lines, etc.). Traditionally, the floor-rupture problem is solved through the use of thicker floor-plates, stronger, tougher and usually heavier material and through the utilization of applique armor. This approach is generally associated with

unnecessarily oversized/overweight vehicle-hull floors and, is being abandoned nowadays due to aforementioned military's requirements for lighter vehicles. Instead, the use of light-weight high-performance polymer-matrix composites in the manufacture of the military-vehicle hull-floors is currently being promoted.

1.3 Detonation of shallow-buried mines

Detonation is a high-rate chemical reaction in which condensed matter explosive is converted into high-pressure, high-temperature expanding gases (commonly referred to as gaseous detonation products). Expansion of the gaseous detonation products against the surrounding medium is associated with exchange of linear momentum and various energy components (e.g. potential, thermal, kinetic, strain, etc.). In the case of detonation of soil-buried land-mines, two extreme scenarios are generally identified:

(1) The so-called "camouflet" scenario in which the mine depth of burial (DOB) is so large that the high potential energy of the detonation products is almost exclusively transformed into inelastic and elastic strain energy of the soil as well as into surface energy of fractured soil particles. In this case, attenuation of the detonation-induced shock waves within the soil is so prevalent that no significant blast wave is generated at the air/soil interface and no soil ejection takes place. In addition, gaseous detonation products remain trapped within the soil. Therefore, in the case of camouflet, structures located at or above the ground are not exposed to any significant threat while underground structures in close proximity can be threatened.

(2) The ground-laid mine detonation scenario in which the impulse energy carried by air-borne shock waves and the kinetic energy of the detonation products pose the main threat to an above-the-ground target structure.

In the majority of situations, mines are shallow-buried in soil and, hence, neither of these extreme scenarios is encountered. While blast waves and detonation products still pose a threat to the target structure, the soil ejecta pose a greater threat. Consequently, the detonation of shallow-buried mines is of main concern to the designers and developers of targeted structures with high blast survivability (e.g. vehicle hull). That is the reason that this regime of mine deployment is discussed in greater detail in the remainder of this sub-section.

The shallow-buried mine detonation process can be described in terms of three well defined temporal phases, Figure 1(a)-(f):

(1) The initial phase, which is characterized by the interaction of high-pressure, high-temperature expanding gaseous detonation products with the surrounding soil. Within this phase, one can typically identify three distinct zones within the soil, the sizes of which scale with the mine characteristic dimension (e.g. radius, R_e). The innermost zone, commonly referred to as the "zone of crushing", extends ca. $2R_e$-$3R_e$. Within this zone the pressures and temperatures are so high that the soil melts/evaporates, rendering knowledge of the material constitutive response irrelevant. The intermediate zone extends between ca. $3R_e$ and $6R_e$, and the soil response to detonation-induced shock loading is dominated by irreversible compaction and crushing/fracturing of the soil particles. The outermost zone extends beyond ca. $6R_e$ and the (attenuated) shock-induced soil response within this zone is dominated by reversible/elastic deformation of the soil. It is generally believed that the initial

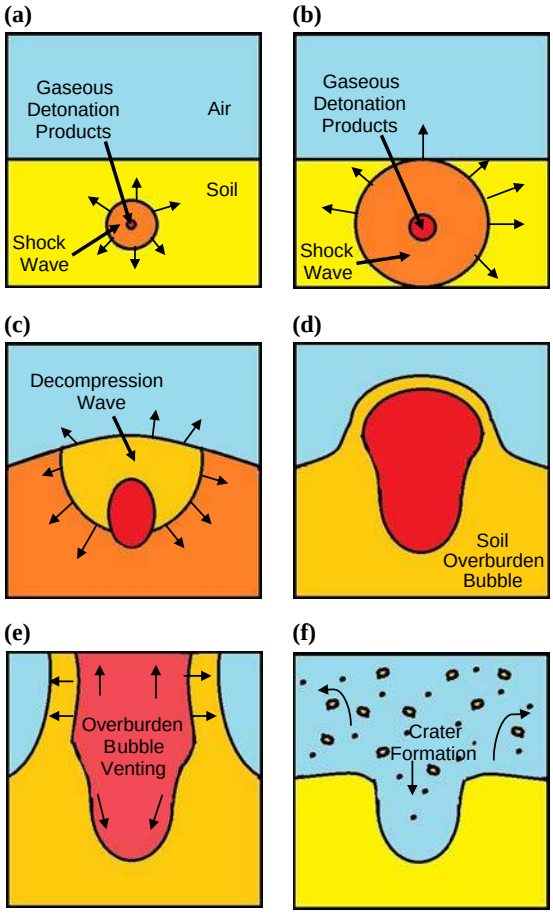

Note: Please see text for details

Figure 1.
Various phases of detonation of a landmine shallow-buried in soil

phase of shallow-buried mine detonation controls the amount of energy available for conversion into soil kinetic energy and, in turn, the extent of threat posed to the targeted structure (e.g. Holsapple and Housen, 2004). Furthermore, the magnitude of the energy available for conversion is affected by factors such as mine shape, mine depth-of-burial, soil properties, etc.

(2) The initial phase ends, and the next phase (commonly known as "soil-overburden bubble initiation phase") begins, at the moment of arrival of the soil-borne shock wave to and the interaction with the soil/air interface. Due to a large shock-impedance mismatch between soil and air, this interaction results in a weak transmitted compressive shock to air and a very strong reflected tensile-shock/release-wave. Under the influence of the tensile-shock/release-wave and the expanding high-pressure detonation products, the soil overburden begins to expand outward, forming (initially) a hemi-spherical dome. This phase typically lasts for a few milliseconds and ends with the moment of rupture of soil overburden and the onset of venting of the detonation products.

(3) The final phase of shallow-buried mine detonation is characterized by gaseous detonation product venting and pronounced soil ejection. Typically, the soil overburden represents only a minor fraction of the total ejected soil. The remaining major portion of the ejected soil is the result of the erosion of the cavity walls by the swirling gaseous detonation products, still residing within the cavity. This interaction gives rise to the formation of a soil crater with a volume many times larger than the volume of the detonated charge. The trajectory of the ejected soil falls within an inverted cone with an included angle (between 60 and 90°). Typically, the included angle varies inversely with DOB and soil initial density.

1.4 Landmine-detonation-induced impulse loading

Detonation of landmines produces large impulsive loads on the targeted vehicle/personnel through impact by the resulting blast waves, ejected soil and expanded gaseous detonation products. Development of military vehicles (and general structural platforms) with a high-level of blast-survivability entails: the understanding of and ability to quantify the impulsive loads associated with the detonation of landmines deployed in soil of differing compositions/constitutions; and the ability to predict the kinematic and structural (including failure) response of the targeted platforms. Acquiring such understanding and predictive ability, however, is typically quite challenging since the detonation-induced loads depend strongly on the deployed mine's shape, size and DOB, the distance between the soil surface and the target (the so-called stand-off distance, SOD), and the soil properties (density, particle size and distribution, presence of inorganic/organic matter, water content, etc.).

Examination of the public-domain literature conducted for the present work revealed a number of scientific papers and technical reports pertaining to the problem of detonation of buried (explosive) charges. Among the reported experimental studies dealing with mine-detonation loading and kinematic/mechanical response of the targeted structure, the following appear to be the most closely related to the subject matter of the current study: Westine *et al.* (1985) conducted a series of experiments using a plate fixtured and centered above a (anti-tank landmine-simulating) buried charge. The plate was perforated at different radial distances and plugs of known mass were placed in the holes. Under the influence of the mine detonation-induced blast loads, the plugs were forced out of the plate and the local impulsive loading on the plate was quantified by measuring the plug velocity; based on the results of Westine *et al.* (1985) and Morris (1993) developed a computer code for design of mass-efficient, blast survivable vehicles/structures; in the work of Bergeron *et al.* (2002), an instrumented ballistic pendulum was utilized to investigate mine detonation-induced loads experienced by a target structure. In addition, this work quantified: the time-dependent pressure and impulse at several locations in air directly above the mine; the time-dependent pressure and impulse at several locations in the sand surrounding the mine; and x-radiographs and high speed photographs of the associated soil cratering and ejection phenomena; and the work of Bergeron *et al.* (2002) was subsequently extended by Braid (2001) who incorporated improved instrumentation along with different charge sizes and soil types.

1.5 Use of computer-aided engineering

Over the last two decades, the use of computational analyses in the design of military vehicles has continuously increased. Efficient computational codes and fast, massive

and inexpensive computational resources enable today computational investigations of whole-vehicle performance under various in-service (e.g. Grujicic *et al.*, 2010a; Grujicic and Bell, 2011b) and threat (e.g. Grujicic *et al.*, 2009a, b, c) conditions. However, the true utility of these computational analyses remains questionable considering that critical shortcomings of these analyses, are either not fully identified or not fully understood. For example, material models used in these analyses need substantial improvements in order to take into account the contribution of various microstructural effects (at various length scales), the effects of components manufacturing and assembly as well as the effects of realistic environmental, thermal, mechanical, and dynamic loading conditions on material behavior (e.g. Grujicic *et al.*, 2009d). In addition, many issues associated with the interactions and contacts between the vehicle and its surroundings (including interactions with fluids and discrete-matter) are still not fully resolved. This situation requires that extensive experimental testing and validation efforts still be employed during development of new or retro fitting of the existing military vehicles. In other words, computational analyses are presently capable of reducing somewhat the new-vehicle development time and of lowering the extent of (but not fully eliminating a need for) the experimental testing and validation efforts.

1.6 Main objectives

The main objective of the present work is to employ a combined finite-element/discrete-particle computational analysis in order to investigate potential benefits and drawbacks associated with material substitution (from steel to composite) in military-vehicle hull-floors whose primary function is to provide the required level of vehicle-occupant protection against blast-loads resulting from the detonation of shallow-buried land-mines.

A review of the public-domain literature carried out as part of the present work revealed that the landmine-detonation-related computational research activities can be broadly divided into three main categories:

(a) shock and blast wave mechanics/dynamics including landmine detonation phenomena and large-deformation/high-deformation rate constitutive models for the attendant materials (high explosive (HE), air, soil, etc.) (e.g. Grujicic *et al.*, 2008b);

(b) the kinematic and structural response of the target to blast loading including the role of target design and use of blast attenuation materials (e.g. Grujicic *et al.*, 2007c); and

(c) vulnerability of human beings to post-detonation phenomena such as high blast pressures, spall fragments and large vertical and lateral accelerations (e.g. Grujicic *et al.*, 2009b).

While the present work falls into the categories (a) and (b) of the research listed above (since it emphasizes both the role of the hull-floor, mine and soil materials, as well as the kinematic and structural responses of the target structure to detonation of landmines shallow buried in soil), it also briefly addresses some of the issues related to category (c).

1.7 Paper organization

A brief description of the problem analyzed in the present work and a brief overview of the computational methods and tools used are provided in Section 2. The main results

obtained in the current work are presented and discussed in Section 3. The main conclusions resulting from the present work are summarized in Section 4.

2. Problem description and computational analysis

As mentioned earlier, the main objective of the present work is to employ a combined finite-element/discrete-particle computational analysis in order to investigate potential benefits and drawbacks associated with material substitution (from steel to composite) in military-vehicle hull-floors whose primary function is to provide the required level of vehicle-occupant protection against blast-loads resulting from the detonation of shallow-buried land-mines. In this section, details are presented regarding the basic problem formulation as well as regarding the computational procedure utilized.

2.1 Problem description

The basic problem analyzed in the present work involves a prototypical buried-mine detonation event followed by the interaction of gaseous detonation products, soil ejecta and blast waves with the target structure, a mock-up of a military-vehicle hull floor to which a distribution of the mass is attached (in order to mimic the presence of the remainder of the military-vehicle). Details regarding the computational model and the numerical procedure employed in the present work to investigate the interaction of the gaseous detonation products, soil ejecta and air-blast-waves with the target structure, and the kinematic/structural response of the target, are presented in subsequent sections.

2.2 Computational domain

The computational domain used consists of two separate sub-domains, one of the continuum Lagrangian-type and the other of a discrete-particle type. The Lagrangian sub-domain comprises the military-vehicle hull-floor (modeled as a rectangular parallelepiped-shaped steel/composite-material plate). This plate is discretized into 90,000 continuum first-order eight-noded reduced-integration elements with a nearly cubic shape. As mentioned earlier, to account for the remainder of the military vehicle, in a highly simplified way, a number of mass and rotary-inertia elements are attached to the hull-floor (from above and below). The values for the mass and moment of inertia of these elements are obtained by dividing a real vehicle into a number of hypothetical sections, treating each section as a rigid body, and calculating the mass properties of each of the sections using the standard procedures. Details regarding the type of vehicle used, the center of mass, and the moment of inertia of each of the segments are not revealed here due to their potential misuse.

As far as the discrete-particle sub-domain is concerned, it comprises mine/detonation-products, sand/soil, and the ambient air. The discrete-particle sub-domain is of a rectangular parallelepiped shape which encloses the hull-floor. Details regarding the discrete-particle modeling and simulations will be presented in the next section.

It should be noted that, due to random distribution of the (detonation-products, soil and air) discrete particles, the computational domain does not possess any axes or planes of symmetry. Nevertheless, it is assumed that the computational domain possesses two vertical planes of symmetry and that the discrete-particle positions in the four resulting quadrants are mutually related through reflection operations across these planes of symmetry. Consequently, only one-quarter of the computational domain had to be analyzed in the present work. It should be noted that, due to the assumed symmetry of the (effectively non-symmetric) computational domain, potential rotation

of the hull-floor/vehicle and motions parallel to the ground could not be analyzed. As shown in our previous work (Grujicic *et al.*, 2009a), when the mine is buried under the center of the vehicle hull-floor, the extent of the non-considered rotational and translational motions is relatively small.

Figure 2 shows an initial configuration of the (quarter) computational domain analyzed. For clarity, the air particles are displayed as smaller spheres.

2.3 Discrete-particle formulation

As mentioned above, the behavior of HE gaseous detonation products, soil and air, following detonation, and during their collision with the hull-floor is modeled in the present work using the discrete-particle (also known as the "corpuscular") approach proposed recently by Olovsson *et al.* (2010). Within this approach, HE gaseous detonation products, soil and air are all represented as assemblies of discrete, rigid, spherical, interacting particles which exchange momentum and kinetic energy during their collisions/contact with each other and/or the hull-floor. To make the computational cost manageable, each particle is defined to represent a collection of 10^{15}-10^{20} molecules.

As explained by Børvik *et al.* (2009, 2011), the discrete-particle method has the following three main advantages over the commonly used combined Lagrangian-Eulerian approaches:

(1) due to its Lagrangian (material-based) character, the method does not require the calculation of the material advection through the mesh and, hence, does not suffer from errors associated with such calculation;

(2) numerical detection and quantification of the contacts and interactions between HE detonation products, soil and air and complex-geometry Lagrangian target structures, which are quite challenging within the combined Lagrangian-Eulerian framework, is greatly simplified and accelerated; and

(3) within the same computational model, HE detonation products, soil and air (all modeled using the discrete-particle approach) can be combined with continuum-Lagrangian-type target structures to analyze various scenarios related to detonation of shallow-buried mines and the interactions of the detonation products, soil ejecta and air-borne blast-waves with the structures.

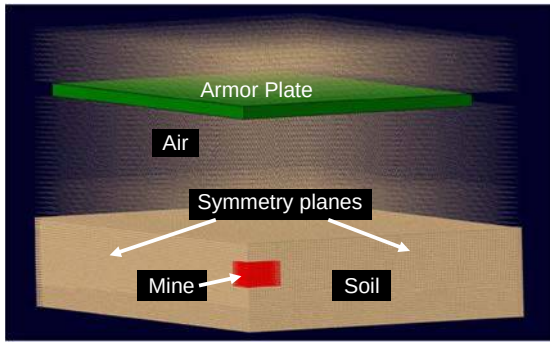

Note: Please note that the mine is shallow-buried and its view is obstructed by the surrounding soil

Figure 2.
A prototypical computational domain used in the combined three-dimensional finite-element/discrete-particle analysis of the buried-mine detonation event and the subsequent interactions of the detonation products, soil ejecta and air blast with the hull-floor

In the remainder of this section, details are presented regarding the discrete-particle models for the HE detonation products, air and soil (with different levels of hydration). It should be noted that, as explained by Olovsson *et al.* (2010), discrete-particle models for the HE detonation products and air are essentially an extension of the kinetic molecular theory of gases, as formulated in 1860 by Maxwell (1860). Specifically: discrete particles used in the numerical model represent a collection of a large number of atoms constituting the material in question; and inter-particle collisions are assumed to be purely elastic (i.e. kinetic-energy-preserving).

Kinetic molecular theory of gases. The kinetic molecular theory is a theory which successfully relates molecular-level events such as collisions to the macroscopic properties, e.g. pressure or temperature of an ideal gas. Within the theory, the system of interacting gas molecules is assumed to have the following four properties:

(1) The size of the molecules is much smaller than the average inter-molecular distance. Consequently, the volume of the molecules is negligible in comparison to the volume of the space within which the gas resides.

(2) The system is in the state of thermodynamic equilibrium, i.e. there is no net flux of mass, linear momentum or energy through the system.

(3) Particle dynamics is governed by Newton's laws of motion.

(4) Inter-molecular and molecule/structure interactions are perfectly elastic and, thus, not only the linear momentum but also the total kinetic energy is preserved.

The kinetic molecular theory was originally proposed by Bernoulli (1738) and Bernoulli and Bernoulli (1968) and further developed by Maxwell (1860). By carrying out a detailed statistical analysis of molecular-level interactions, Maxwell was able to derive the following (often referred to as the Maxwell-Boltzmann) expression for the equilibrium molecular velocity distribution function, $f(v)$:

$$f(v) = 4\pi\left(\frac{M}{2\pi RT}\right)^{3/2} v^2 \exp\left(\frac{-Mv^2}{2RT}\right) \tag{1}$$

where M is the molar mass, R is the universal gas constant and T is the absolute temperature.

Based on Equation (1), Maxwell derived the root-mean-square (rms) molecular velocity, v_{rms}, as:

$$v_{rms} = \sqrt{\int_0^\infty v^2 f(v) dv} = \sqrt{\frac{3RT}{M}} \tag{2}$$

Under a condition that the gas molecules, modeled as spherical particles, possess a finite radius r_p, additional important quantities characterizing molecular-level interactions within an ideal gas include the mean-free-path, l, and frequency of collisions, f_c, defined as:

$$l = \frac{1}{\sqrt{2}\pi n r_p^2} \tag{3}$$

and:

$$f_c = nr_p^2\sqrt{\frac{8\pi RT}{M}} \tag{4}$$

where n is the number of molecules per unit volume.

Within the kinetic molecular theory of gases, the pressure is the result of the collisions of the molecules with the surroundings. By computing an average rate of change of the momentum per unit area of the surroundings, Maxwell was able to derive the following expression for pressure, p:

$$p = \frac{2}{3}e_t = \frac{m}{3V}\sum_{i=1}^{N} v_i^2 = \frac{mN}{3V}v_{rms}^2 \tag{5}$$

where e_t is the translational kinetic energy per unit volume, m is the molecular mass, V is the volume of the system and N is the number of molecules in the system.

HE gaseous detonation products. The constitutive and the dynamic response of HE gaseous detonation products is represented using the discrete-particle material model proposed by Olovsson *et al.* (2010). Since a detailed overview of this model could be found in Olovsson *et al.* (2010), only a brief account of it is given below. Complete parameterization of the HE discrete-particle model requires specification of the following four quantities:

(1) initial mass density, $\rho_{O,HE}$;

(2) initial volumetric internal energy density, $E_{O,HE}$;

(3) constant-pressure to constant-volume heat-capacity ratio $\gamma_{HE} = C_{p,HE}/C_{v,HE}$; and

(4) fraction of the total volume occupied by the discrete particles, b_{HE}.

The four parameters are used to set up a discrete-particle computational model in the following way: first, once the number of molecules per particle N_{mpp} is selected, $\rho_{O,HE}$ is used to determine the number of particles in the computational volume N_p; second, since γ_{HE} controls partitioning of the total specific kinetic energy ($E_{O,HE}/V = e_{t,HE} + e_{s,HE}$) into its translational, $e_{t,HE}$, and rotational/vibrational, $e_{s,HE}$, components as:

$$\frac{e_{s,HE}}{e_{t,HE}} = \frac{5 - 3\gamma_{HE}}{3\gamma_{HE} - 3} \tag{6}$$

$e_{t,HE}$ and $e_{s,HE}$ could be determined from the given $E_{O,HE}$ and γ_{HE} for a system of a given volume V; and third, the extent of the so-called "co-volume" effect (discussed below) is controlled by the magnitude of b_{HE}.

Børvik *et al.* (2011) pointed out that the kinetic molecular theory-based expression for pressure, Equation (5), typically under-predicts pressure levels at extremely high densities encountered in HE detonation products. The reason for this breakdown is the fact that at such high density levels, the volume of the molecules (the so-called "co-volume" effects) could not be neglected (as is done in the case of the kinetic molecular theory). To account for the co-volume effects (Baibuz *et al.*, 1986; Clausius,

1880), the radius/size of the HE discrete particles is adaptively increased within the present computational approach. This correction is similar to the van der Waals co-volume correction of the ideal gas pressure, Equation (5), which involves division of the right-hand side of Equation (5) by a factor $(1-b_{HE})$. In addition to the aforementioned inability of the kinetic molecular theory to accurately predict pressure at high densities, this theory also fails to account for the experimentally observed sharp drop in pressure during adiabatic expansion of the HE detonation products. To overcome this problem, Olovsson *et al.* (2010) suggested that γ_{HE} be changed from its prototypical value of 7/5 for a di-atomic gas to its maximum theoretical value of 5/3 (i.e. to the value found in a mono-atomic gas). The effect of adiabatic expansion from state 1 to state 2 is described by the following ideal gas relation:

$$\frac{p_2}{p_1} = \left(\frac{V_2}{V_1}\right)^{-\gamma} \tag{7}$$

This relation reveals how increasing γ_{HE} from 7/5 to 5/3 increases the rate of adiabatic expansion pressure drop. It should be noted that, as pointed out above, γ_{HE} controls the $e_{s,HE}/e_{t,HE}$ ratio and according to Equation (6), for $\gamma_{HE}=5/3$ this ratio becomes zero. In other words, the total internal energy becomes equal to the kinetic/translational energy (i.e. zero rotational/vibrational kinetic energy is assigned to the HE discrete particles).

In order to parameterize the discrete-particle model for the HE, one must first choose the type/grade of HE. In the present work, C-4 HE is selected. For the discrete-particle HE model to be considered realistic, it must reproduce some of the basic findings obtained using experimental and/or purely continuum-type computational approaches. Within the continuum framework, the behavior of HE detonation products is commonly represented using the so-called "equation of state" (EOS), a function relating the pressure to the material mass-density/specific-volume and mass-based internal-energy-density/temperature. Typically, either the Jones-Wilkins-Lee (JWL) or the ideal gas EOS is used.

As pointed out by Børvik *et al.* (2011), parameterization of the C-4 discrete-particle model can be carried out by stipulating that the aforementioned requirement is fulfilled. Specifically, Børvik *et al.* (2011) systematically varied the C-4 discrete-particle model parameters within an optimization scheme in order to match the experimental (as well as the continuum-level modeling) results of the so-called "cylinder test" (Souers *et al.*, 1996; Souers, 2007). Within the cylinder test, an oxygen free high conductivity (OFHC) copper pipe is filled with an HE and the explosive is detonated at one end. This causes the formation of a (transverse) detonation wave and its propagation along the length of the pipe. By monitoring the temporal evolution of the pipe radial displacement/velocity and its spatial distribution along the pipe length, properties of the explosives can be determined and quantified as the parameters of the postulated EOS. For example, for C-4 and the assumed JWL EOS in the form:

$$p = A\left(1-\frac{\omega}{R_1 V_{HE}}\right)e^{-R_1 V_{HE}} + B\left(1-\frac{\omega}{R_2 V_{HE}}\right)e^{-R_2 V_{HE}} + \omega E_{HE} \tag{8}$$

where p is the pressure, $V_{HE}=\rho_{HE}/\rho_{0,HE}$, E_{HE}/V is the volumetric internal energy density, there are five JWL EOS material-model parameters (A, B, ω, R_1, R_2). These

parameters were determined by Børvik *et al.* (2011) using an optimization algorithm coupled with the combined Lagrangian-Eulerian finite-element analysis of the cylinder test and the experimental cylinder-test data by Souers *et al.* (1996). A list of the values for these parameters can be found in table 1 of Børvik *et al.* (2011).

To parameterize the C-4 discrete-particle material model, Børvik *et al.* (2011) carried out combined finite-element/discrete-particle simulations within which the OFHC pipe is treated as a continuum-Lagrangian finite-element discretized component (modeled using the Johnson-Cook linear-elastic/strain-hardening/rate-dependent/thermally softenable-plastic constitutive equation (Frutschy and Clifton, 1998)) while C-4 is represented as an ensemble of 1,000,000 discrete particles. Next, within an optimization study, the discrete-particle model parameters are varied systematically until the resulting temporal evolutions and spatial distributions of the pipe radial displacement/velocity (caused by the explosive detonation initiated at one end of the pipe) match the same experimental results as those used for parameterization of the C-4 JWL EOS. The procedure employed by Børvik *et al.* (2011) yielded the following C-4 discrete-particle material-model parameters: $\rho_{0,HE} = 1{,}601\,\mathrm{kg/m^3}$; $E_{0,HE}/V = 8.7\,\mathrm{GJ/m^3}$; $\gamma_{HE} = 7/5$; and $b_{HE} = 0.35$. It should be noted that the values for $\rho_{0,HE}$ and $E_{0,HE}/V$, as well as the detonation velocity $D = 8{,}190\,\mathrm{m/s}$, were taken directly from the JWL-EOS C-4 parameterization carried out by Souers *et al.* (1996). In other words, parameter-optimization was carried out only for γ_{HE} and b_{HE}.

Air. Air surrounding the target structure and located above the soil is treated as a diatomic ideal gas initially at the ambient pressure (101.3 kPa) and reference temperature (298 K). Following Børvik *et al.* (2011), the four basic discrete-particle model parameters are assigned the following values: $\rho_{0,\mathrm{air}} = 1.184\,\mathrm{kg/m^3}$; $E_{0,\mathrm{air}}/V = 0.25325\,\mathrm{MJ/m^3}$; $\gamma_{\mathrm{air}} = 7/5$; and $b_{\mathrm{air}} = 0$ (no co-volume effects considered). Following the same procedure as in the case of HE detonation products, these parameters are used to determine, at the onset of simulation, the number of the air discrete particles and partitioning of the total internal energy into its kinetic translational and kinetic rotational/vibrational parts. It should be noted that in this case, $e_{s,\mathrm{air}}/e_{t,\mathrm{air}} = 2/3$ and $e_{s,\mathrm{air}}$ is not zero any longer. However, while in an ideal-gas molecular system, $e_{s,\mathrm{air}}/e_{t,\mathrm{air}}$ acquires this equilibrium value only in a statistical sense, within the present discrete-particle model, the ratio is imposed on each individual particle to reduce the computational cost. It should be further noted that, within the present discrete-particle model for air, $e_{s,\mathrm{air}}$ is treated as a scalar variable, i.e. no explicit consideration is given to the rotational/vibrational degrees of freedom of the particles. Since the collision of two air particles is of an elastic character, the momentum and the total kinetic/internal energy are conserved, as well as the $e_{s,\mathrm{air}}/e_{t,\mathrm{air}}$ ratio. These conditions are used to determine particle velocities following collision. As far as the collision between an air particle and an movable/deformable structure is concerned, the exchange of the kinetic translational energy between the particle and the structure causes the $e_{s,\mathrm{air}}/e_{t,\mathrm{air}}$ ratio to depart from its equilibrium value until the particle in question collides with another particle.

It is important to recognize that the constancy of $e_{s,\mathrm{air}}/e_{t,\mathrm{air}}$ ratio corresponds to the assumption of thermal equilibrium within air. This assumption is justified for air prior to detonation. However, upon detonation, linear momentum transfer from the HE detonation products to air causes the air-molecules/discrete-particles to acquire very large values of their kinetic translational energy (i.e. the condition of thermal equilibrium does not hold any longer).

Soil. While the soil is also modeled using a discrete-particle approach, the soil discrete-particle model differs from those used for the HE gaseous detonation products and air in that soil particle collisions are modeled using a penalty rather than an elastic (or, more precisely, kinematic-elastic) collision algorithm. This was done in order to account for the effects such as: soil-particle finite stiffness; rate-dependent dissipative/damping nature of the inter-particle collisions; and the inter-particle frictional effects.

The essential features of the penalty contact used are depicted schematically in Figure 3 which shows a two-particle contact model. Within this model, particle normal interactions are accounted for by a linear spring (with a spring constant k) and a linear dashpot (with a damping coefficient c) connected in parallel. As far as the tangential interactions are concerned, they are modeled using a linear spring (also of stiffness k) and a Coulomb frictional element (which is characterized by a friction coefficient μ and which limits the tangential-spring force). It should be noted that soil-particle fracture processes are not considered since they are associated with minor energy absorption/dissipation effects and, hence, are not expected to significantly affect the computational results. Furthermore, it should be noted that the soil-particle stiffness is not accounted for explicitly since the particles are of a rigid type. Rather, through the proper selection of the stiffness constants of the normal and tangential contact springs, particle stiffness is accounted for implicitly.

As in the case of the HE/air discrete-particle models, only the translational degrees of freedom are considered in the case of the soil discrete-particle model (in order to reduce the computational cost). A limited number of computational analyses in which the rotational degrees of freedom were included show that the results obtained are not greatly affected by the inclusion of soil-particle rotations while the computational cost was greatly increased.

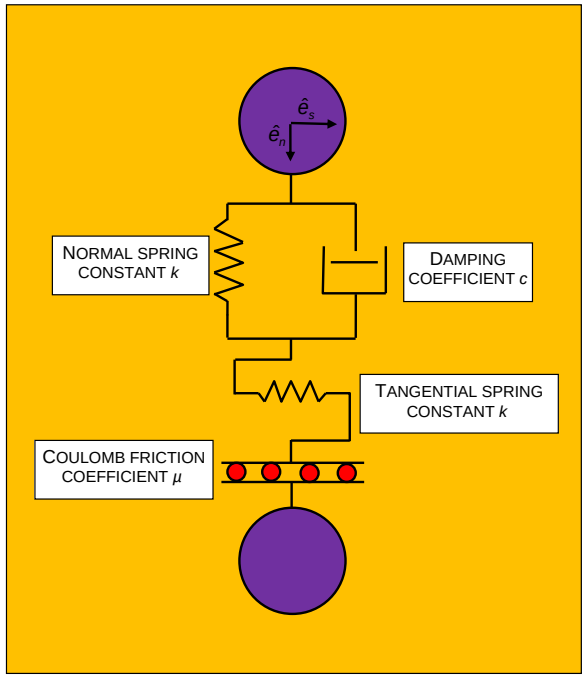

Figure 3.
A schematic of the contact-mechanics model involving two interacting equal-sized/mass spherical particles of soil

In the present work, both the cases of dry and saturated soil/sand are considered. In the remainder of this section, details are presented regarding the discrete-particle model parameterization for the cases of dry and saturated soil.

Dry soil. Dry soil is represented using constant radius rigid spherical particles with the particle-material density of 2,700 kg/m^3 and the initial particle volume fraction of 0.6 (yielding the soil initial density of 1,620 kg/m^3). To fill the soil sub-domain with the particles and to parameterize the contact model, the following three-step procedure is used:

(i) The soil sub-domain is first assumed to be a three-dimensional array of identical unit cells with the periodic boundary conditions being applied across the faces of the unit cells. To determine the initial distribution of the soil particles within the unit cell, the number of particles required to attain a volume fraction of 0.6 are placed in the unit cell while ensuring that no inter-particle penetration takes place. An example of a prototypical soil unit cell is displayed in Figure 4.

(ii) Next, the unit cell is subjected to volumetric compression, and the particle contact stiffness k and the contact damping coefficient c are varied in a systematic manner (while holding the inter-particle friction coefficient at a constant level of $\mu = 0.15$ (Grujicic *et al.*, 2010b, 2011a)) until a good match is obtained between the experimentally measured (for prairie sand containing high level of silt and clay) pressure vs density and the computed pressure vs density functional relations. More details of this procedure can be found in our recent work (Grujicic *et al.*, 2013b). This procedure yielded $k = 4$ GN/m, $c = 0.0$ MN.s/m, and $\mu = 0.15$. The hydrostatic pressure within the unit cell is computed by dividing the average force experienced by the unit cell faces by the face surface area.

(iii) The soil sub-domain is constructed by partitioning it into a three-dimensional array of unit cells and filling each cell identically using the particle configuration obtained in (i).

Saturated soil. In the case of saturated soil, water is not modeled explicitly. Instead, its effect on the distribution and the mechanical response of the soil-particle assembly is accounted for implicitly. Specifically: while keeping the soil-particle size uniform and the particle volume fraction ($= 0.6$) the same as in the case of the dry soil, the weight

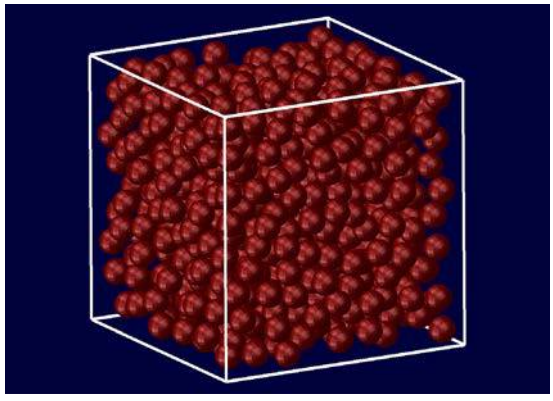

Figure 4.
Prototypical soil unit cell used in the present combined finite-element/ discrete-particle computational analysis of mine detonation and interaction of the detonation products, soil ejecta and air blast with the hull-floor

of water is accounted for by increasing the saturated-soil density to $(0.6 \times 2{,}700) + (0.4 \times 1{,}000) = 2{,}020\,\text{kg/m}^3$ (yielding the saturated soil-particle effective material density of $2{,}020/0.6 = 3{,}367\,\text{kg/m}^3$); to account for an increase in the fully compacted soil density typically observed in saturated soil, increased particle packing (particle volume fraction = 0.64) was achieved by allowing ± 2.5 percent variations in the soil-particle diameter and by taking advantage of the fact that higher densities are obtained in a system containing particles of non-uniform size. Using the same procedure as above, this yielded the saturated-soil density of $(0.64 \times 2{,}700) + (0.36 \times 1{,}000) = 2{,}088\,\text{kg/m}^3$ and the saturated soil-particle material density of $2{,}088/0.64 = 3{,}262\,\text{kg/m}^3$; and inter-particle contact stiffnesses, damping and friction coefficients were adjusted to account for the effect of water by utilizing the aforementioned procedure (Grujicic *et al.*, 2013b). Specifically, the damping coefficient:

$$c = 2\xi\sqrt{mk} \tag{9}$$

is adjusted (by varying the damping ratio ξ, i.e. the ratio of the damping coefficient and the critical damping coefficient) to match the experimental observations (Deshpande *et al.*, 2009) that in wet sand, reflection of a compressive shock wave from the soil/air interface does not produce a loose spray of soil particles (an indication of a weaker reflected tensile shock and an increased inter-particle cohesion). This procedure in conjunction with the saturated soil experimental pressure vs density data (Grujicic *et al.*, 2007a, 2009e) yielded $k = 40\,\text{GN/m}$, $\xi = 0.025$ and $\mu = 0.01$.

Selected discrete-particle size-based scaling. While keeping the number of soil particles per unit cell constant, the total number of soil particles in the model can be adjusted by changing the unit cell size. However, it should be noted that the discrete-particle model parameters for soil are particle-/unit-cell-size dependent and, hence, changes in the particle size have to be accompanied by the appropriate changes in the discrete-particle model parameters. Specifically: the particle-particle contact stiffness k scales (linearly) with the particle-/unit-cell-size or dimensions; and under the assumption that the damping ratio is particle-size independent, the damping coefficient c, in accordance with Equation (9), is seen to scale with the squared particle size.

2.4 Computational analysis-type

The mine-blast event and the subsequent interactions between the detonation products, soil ejecta and air blasts with the hull-floor are analyzed computationally using a finite-element/discrete-particle algorithm. It should be noted that both the discrete-particle and the continuum portions of the computational domain are of a Lagrangian character (i.e. the particle geometry and the finite-element mesh are each attached to the underlying material). Heat dissipation associated with plastic deformation and damage/failure of the hull-floor is treated as a heat-source. Due to the extremely short duration of the mine-blast detonation event (ca. tens of milliseconds), heat conduction analysis is not carried out. Rather, the purely mechanical analysis is conducted under adiabatic conditions. The effects of local changes in temperature due to adiabatic heating are accounted for through the use of temperature-dependent hull-floor-material properties.

2.5 Initial conditions

Prior to the beginning of the computational analysis, the continuum-Lagrange sub-domain is occupied by the hull-floor, while the respective parts of the

discrete-particle sub-domain are filled with HE detonation products, soil and the ambient air. The continuum-Lagrangian hull-floor sub-domain is assumed to be initially stress-free and stationary.

Filling of the discrete-particle sub-domains with air, soil and detonation products was done in the following way; Air: for the selected number of air molecules per discrete particle, $N_{mpp,\mathrm{air}}$, and the known values of $\rho_{0,\mathrm{air}}$ and V_{air}, the number of air discrete particles, $N_{p,\mathrm{air}}$, is computed. These particles are placed randomly within the air computational sub-domain. Next, random velocities are initially assigned to the air particles by sampling the Maxwell-Boltzmann distribution function, Equation (1), with $M_{\mathrm{air}} = 29$ g/mol and $T_{\mathrm{air}} = 298$ K, while ensuring that the v_{rms} of the air discrete-particle model is identical to that found in the ideal gas, ca. 506 m/s, as modeled by the kinetic molecular theory, Equation (2). This condition ensures that the discrete-particle air pressure ($= 101.3$ kPa) is consistent with $E_0/V = 0.25325$ MJ/m^3 and $\gamma_{\mathrm{air}} = 7/5$, in accordance with the ideal gas law; Soil: as far as the soil sub-domain is concerned, it is constructed, as mentioned earlier, by partitioning it into a three-dimensional array of unit cells and filling each unit cell identically while ensuring that no "penetration" (other than the one caused by gravity) exists between the neighboring particles; and HE detonation products: in the case of HE, initially stationary particles of undetonated explosive charge are placed randomly within the HE discrete-particle sub-domain following a procedure identical to that used in the case of air particles. Next, the explosive charge is detonated. Within the discrete-particle framework, HE detonation is simulated in the following way. At $t = 0$ (the detonation time), with the exception of the HE located at the detonation point(s), the explosive is assumed to be in the solid state and, as mentioned above, the HE discrete particles are assumed to be at rest (more precisely, to have a zero average translational velocity). As the detonation front expands, increasingly more HE is detonated, i.e. converted into the gaseous state due to arrival of the detonation front. Once this solid-gas conversion takes place in a region, the HE particles are assigned a velocity by randomly sampling the Maxwell-Boltzmann thermal velocity distribution function, Equation (1) (Maxwell, 1860), consistent with the $\rho_{C\text{-}4} = 1.82$ g/cm^3, $M_{C\text{-}4} = 222$ g/mol and $T_{C\text{-}4} =$ ca. 3,500 K, where detonated C-4 is treated as monoatomically decomposed RDX, $C_3H_6N_6O_6$. The sampled velocities are next corrected by dividing them with $(1-b_{C\text{-}4})^{1/2}$ in order to account for the aforementioned co-volume-induced pressure increase.

2.6 Boundary conditions

Over the portions of the computational-domain external surfaces initially associated with air and soil, an external/ambient pressure of 101.3 kPa is applied so that particles arriving at the boundary and associated with a local pressure exceeding the external pressure are allowed to leave the computational domain. On the other hand, particles which arrive at the external boundary and are associated with a sub-ambient local pressure are reflected back into the domain.

2.7 Contact algorithms

As mentioned earlier, soil/soil particle interactions are modeled using a (viscoelastic/frictional normal/tangential) penalty contact algorithm. On the other hand, HE/HE, air/air, HE/air, soil/HE and soil/air particle interactions are modeled using an elastic/kinematic contact algorithm.

As far as discrete-particle/hull-floor interactions are concerned, they are modeled using a penalty-contact algorithm. Within this algorithm, contact kinematic

constraints are enforced by ensuring that the extent of contact pressure is governed by the local surface penetrations (where the default penalty stiffness parameter is automatically maximized subject to stability limits). As far as the shear stresses are concerned, they are transferred via a "slip/stick" algorithm, that is, shear stresses lower than the frictional shear stress are transferred without interface sliding (otherwise interface sliding takes place). The frictional shear stress is defined by a modified Coulomb law within which there is an upper limit to this quantity (set equal to the shear strength of the continuum-Lagrange hull-floor sub-domain material). The frictional shear stress is then defined as the smaller of the product between the static/kinetic friction coefficient and the contact pressure, on the one hand, and the Lagrangian sub-domain material shear strength, on the other.

2.8 Material models

As mentioned earlier, selected portions of the discrete-particle sub-domain are filled with HE detonation products, soil and air. The constitutive models for these three materials, within the discrete-particle framework, have been presented in Section 2.3. It should be recalled that while discrete-particle representation of these three materials is based on rigid particles, material's deformability has been recovered through the use of the appropriate contact algorithms. As far as the continuum-Lagrangian hull-floor sub-domain is concerned, it was modeled as a deformable structure made of either a Kevlar®-fiber reinforced poly-vinyl-epoxy-matrix composite or AISI 4340 steel. The deformation and failure constitutive response of these materials are represented using the composite-material model recently presented in Yen (2012) and Grujicic *et al.* (2011c, d, 2013a), and the Johnson-Cook material model, respectively. A brief overview of these material models has been deferred to Appendices 1 and 2.

2.9 Computational algorithm

The governing mass, linear momentum and energy conservation equations are solved with a second-order accurate explicit combined finite-element/discrete-particle algorithm. All the calculations in the present work are carried out by combining a general-purpose mathematical program MATLAB (The MathWorks Inc., 2013) with ABAQUS/Explicit 6.13, a general-purpose finite-element program from Dassault Systèmes (2013). MATLAB was used to create the geometrical/meshed models and ABAQUS input files, as well as to guide ABAQUS-simulation structure and execution, as well as input/output communications.

2.10 Computational accuracy, stability and cost

A standard particle-size and mesh-refinement sensitivity analysis was carried out (the results not shown for brevity) in order to ensure that a convergence of the key results is reached with respect to the further variations of these geometrical/mesh parameters. Due to the conditionally stable nature of the explicit finite element analysis used, the maximum time increment during each computational step had to be kept lower than the attendant stable time increment. A typical 50 ms computational analysis followed by a detailed post-processing data reduction procedure required on average six hours of (wall-clock) time on a 12-core, 3.0 GHz machine with 16 GB of memory.

3. Results and discussion

The combined finite-element/discrete-particle computational model and analysis presented in the previous section are utilized in the present section to assess the

potential benefits and limitations associated with steel-to-composite material substitution in military-vehicle hull-floors.

3.1 Materials spatial distribution and temporal evolution

Spatial distributions of three attendant materials (soil, mine and steel) for the case of steel hull-floors at four different post-detonation times (0.2, 0.5, 0.8 and 1.1 ms) are depicted in Figure 5(a)-(d). Air particles are not shown in these figures for improved clarity. For the same reason, only 1/64th of the soil and mine particles are displayed and the displayed particles are shown with a larger radius than their real radius. Examination of the results displayed in Figure 5(a)-(d) reveals that upon arrival of the ejected soil and mine-detonation-product particles at the bottom face of the hull-floor, the floor experiences upward movement (due to the momentum transfer), substantial upward bulging in its central portion (as a result of extensive deformation), and ultimate rupture (in the same highly deformed region). As a result of the floor-rupture, soil particles can enter the space above the floor-plate (i.e. the cabin space) and floor fragments with an upward momentum are released into the cabin interior.

Spatial distributions of three attendant materials (soil, mine and composite-material) for the case of composite-material hull-floors, at the same four post-detonation times as in the case of the steel hull-floor, are depicted in Figure 6(a)-(d). Examination of the results displayed in Figure 6(a)-(d) and their comparison with the corresponding results displayed in Figure 5(a)-(d) reveals a similar sequence of events as that described above for the case of the steel hull-floor. The main differences are observed relative to the larger extent of damage/rupture and the larger upward

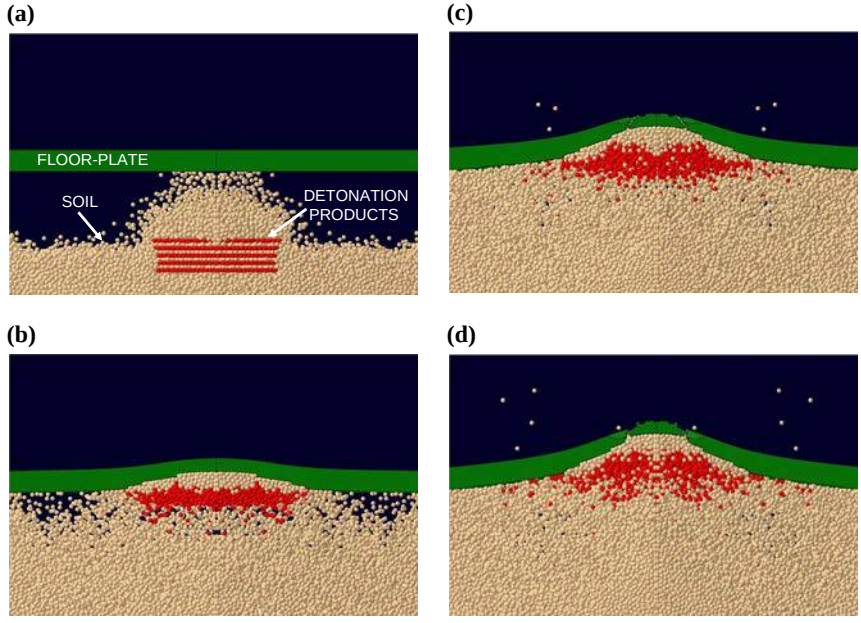

Notes: (a) 0.2 ms; (b) 0.5 ms; (c) 0.8 ms; (d) 1.1 ms. For improved clarity, only 1/64th of the soil and mine particles are displayed and the displayed particles are shown with a larger radius than their real radius

Figure 5.
Spatial distributions of soil, mine and steel for the case of steel hull-floors at four different post-detonation times

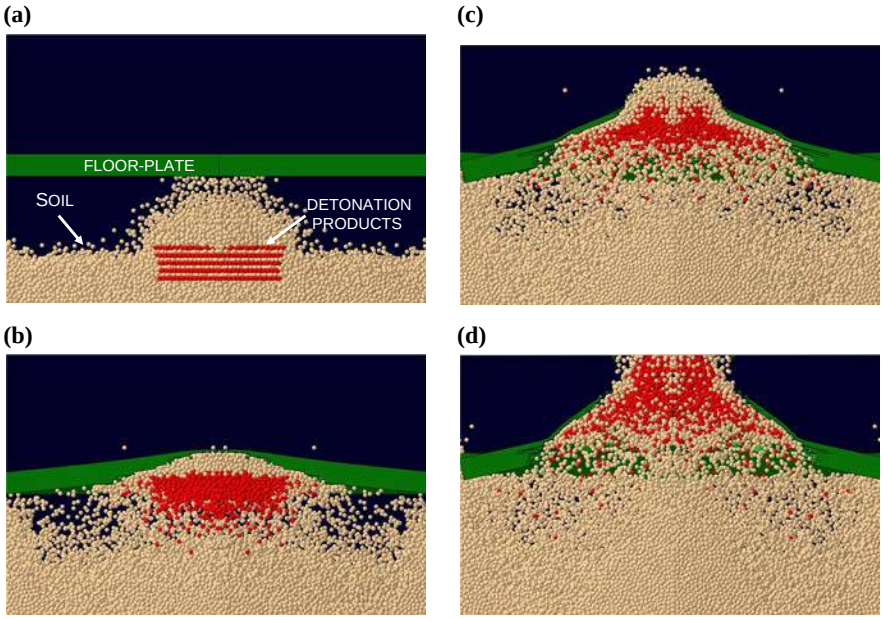

Figure 6.
Spatial distributions of soil, mine and composite-material for the case of composite-material hull-floors at four different post-detonation times

Notes: (a) 0.2 ms; (b) 0.5 ms; (c) 0.8 ms; (d) 1.1 ms. For improved clarity, only 1/64th of the soil and mine particles are displayed and the displayed particles are shown with a larger radius than their real radius

displacement of the composite hull-floor. It should be noted that the two cases of hull-floor analyzed in Figures 5(a)-(d) and 6(a)-(d) are associated with the same plate thickness and, thus, the steel hull-floor is substantially heavier than the composite one.

In the remainder of this section, the two hull-floor cases will be analyzed not under the same floor-thickness condition, but rather with respect to their mass-efficiency relative to the ability of the hull-floor to survive a mine-blast without rupture.

3.2 Composite-to-steel relative mass efficiency

The main concern related to the vehicle-underbelly buried-landmine detonation, as mentioned earlier, is the rupture of the hull-floor. In principle, such a mine-detonation event is characterized by the mass/shape of the landmine, explosive-type, DOB, SOD, etc. In addition, for each such event, there will be, for a given hull-floor material, a minimum critical thickness (or more precisely areal-density), of the hull-floor at which floor rupture will not take place. The lower is the value of this material-specific minimum critical thickness (or areal-density), the more mass-efficient is the hull-floor material in preventing floor rupture.

Figure 7(a)-(d) provide a series of contour plots in which "critical" mass efficiencies of the composite-material and AISI 4340 steel used in the hull-floor are compared. In each of these figures, the mine mass is plotted along the x-axis, DOB (measured with respect to the top surface of the mine) along the y-axis, while the contour lines show the ratio of the critical areal-densities of the composite-material and the steel. The reciprocal of this ratio is a measure of the composite-to-steel relative mass efficiency. In other words, provided this ratio is <1.0, the smaller is its value, the higher are the

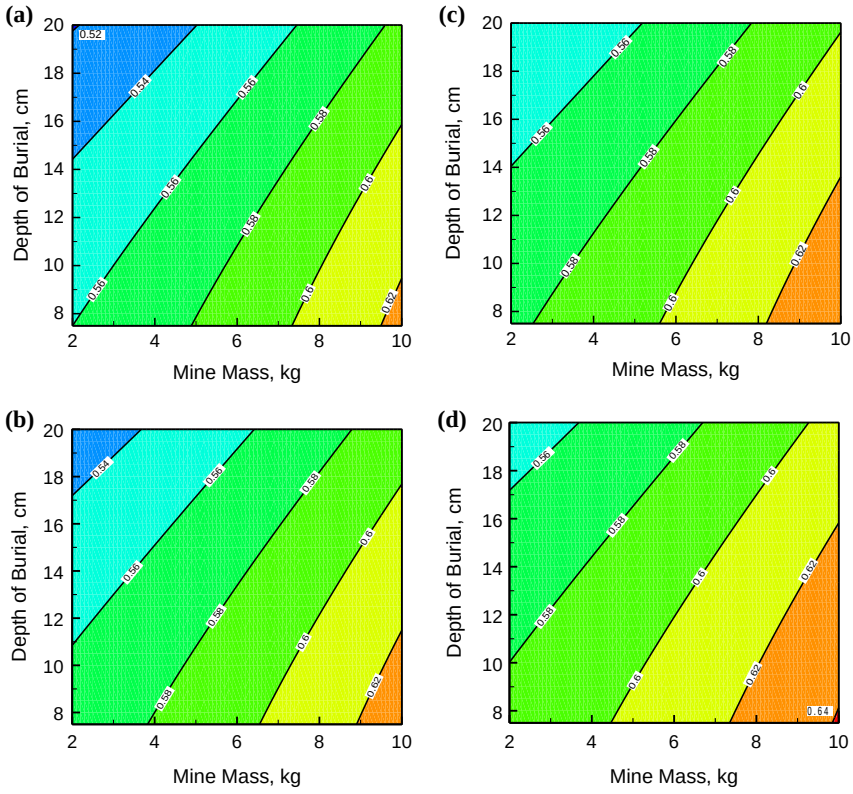

Notes: (a) 40 cm; (b) 60 cm; (c) 80 cm; (d) 100 cm

Figure 7.
The effect of landmine-mass and depth of burial on the ratio of the critical areal-densities of the composite-material and AISI 4340 steel used in the hull-floor, at four stand-off distances

benefits of steel-substitution with a composite material. It should be noted that in Figure 7(a)-(d), the SOD is set to 40, 60, 80 and 100 cm, respectively. Furthermore, in the analysis used to generate the results plotted in these figures, as well as in the figures in the remainder of this section and Sections 3.3-3.5, the following entities/quantities were held constant: the explosive, C-4; mine shape, circular disk; mine diameter-to-height ratio, fixed as 3; and soil condition, dry. In Section 3.6, conditions (a)-(c) will be maintained, while the soil condition will be changed from dry to saturated.

Examination of the results displayed in Figure 7(a)-(d) suggests that the substitution of steel with a composite-material for the hull-floor can result in significant mass reductions, particularly under landmine-detonation scenarios involving low-mass buried charge, large DOB, and low SOD. This conclusion is based on the following specific observations:

(1) the composite-material considered is more mass-efficient than its steel counterpart, i.e. the reciprocal of the composite-to-steel relative mass efficiency is <1.0, for all the landmine-detonation scenarios analyzed;

(2) the overall range of the reciprocal of the composite-to-steel relative mass efficiency is approximately 0.52-0.64;

(3) the ratio of the composite-to-steel areal-densities, at a given level of the SOD, increases with an increase in the landmine mass, and with a decrease in the DOB; and

(4) as the SOD increases, the ratio of the composite-to-steel areal-densities increases monotonically, but moderately.

It is important to note that, since the composite-material considered is less dense than steel (1,783 vs 7,850 kg/m^3), the improved relative mass-efficiency of the composite-material is associated with a thicker hull-floor. An excessively thick hull-floor may become a problem since it will have to be accommodated by reducing the vehicle ground-clearance, the cabin space, or both. To investigate this potential problem, the results pertaining to the ratio of the critical thicknesses of the composite-material and steel hull-floors are depicted as contour plots in Figure 8(a)-(d). Quantities plotted along the *x*- and *y*-axes, as well as the parameter varied between parts (a)-(d), are all identical to their counterparts used in Figure 7(a)-(d). Examination of the results displayed in Figures 8(a)-(d) shows that: depending on the landmine-detonation scenario, the critical thickness (i.e. the minimum thickness which prevents hull-floor rupture) of the composite-material hull-floor is approximately 2.3-2.8 times larger than its steel counterpart; the aforementioned effects of the landmine mass, DOB and SOD on the

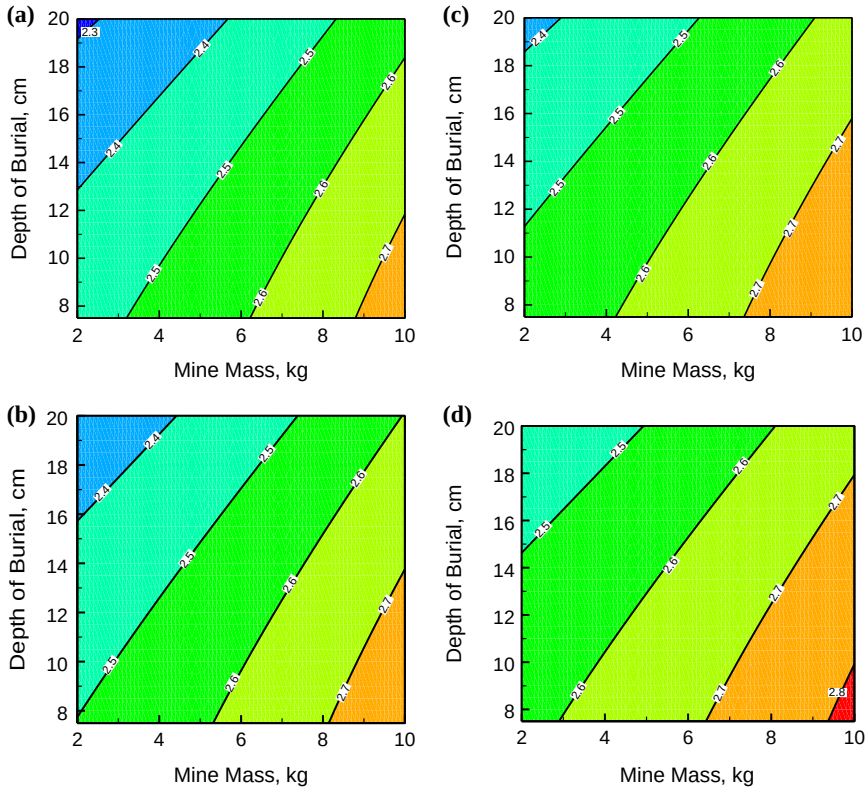

Figure 8.
The effect of landmine-mass and depth of burial on the ratio of the "critical" thicknesses of the composite-material and AISI 4340 steel used in the hull-floor, at four stand-off distances

Notes: (a) 40 cm; (b) 60 cm; (c) 80 cm; (d) 100 cm

relative mass-efficiency are essentially analogous in the case of the critical thickness ratio; and the problem associated with excessive thickness of the composite hull-floor may arise in situations in which the critical thickness of the steel hull-floor is the highest. These conditions are generally associated with the largest landmine mass (i.e. with the maximum detonation-energy released) and intermediate values of the DOB (i.e. the values at which the thickness of the soil overburden is large enough to provide sufficient soil mass for effective momentum transfer to the target, and yet not too high to promote camouflet effects).

3.3 Maximum acceleration consideration

It has been generally recognized that the maximum mine-detonation-induced acceleration of the vehicle (or, more specifically, of its hull-floor) is one of the key blast-variables which must be monitored/controlled since it is believed to correlate with the extent of occupants' injury in the case when hull-floor rupture does not take place. Consequently, the maximum acceleration of the hull-floor top surface is monitored as a function of the aforementioned mine-detonation parameters, and compared between the composite-material and steel hull-floor cases. The results obtained are depicted as a series of contour plots in Figure 9(a)-(d). Quantities plotted along the *x*- and *y*-axes, as well as the parameter varied between parts (a)-(d), are all

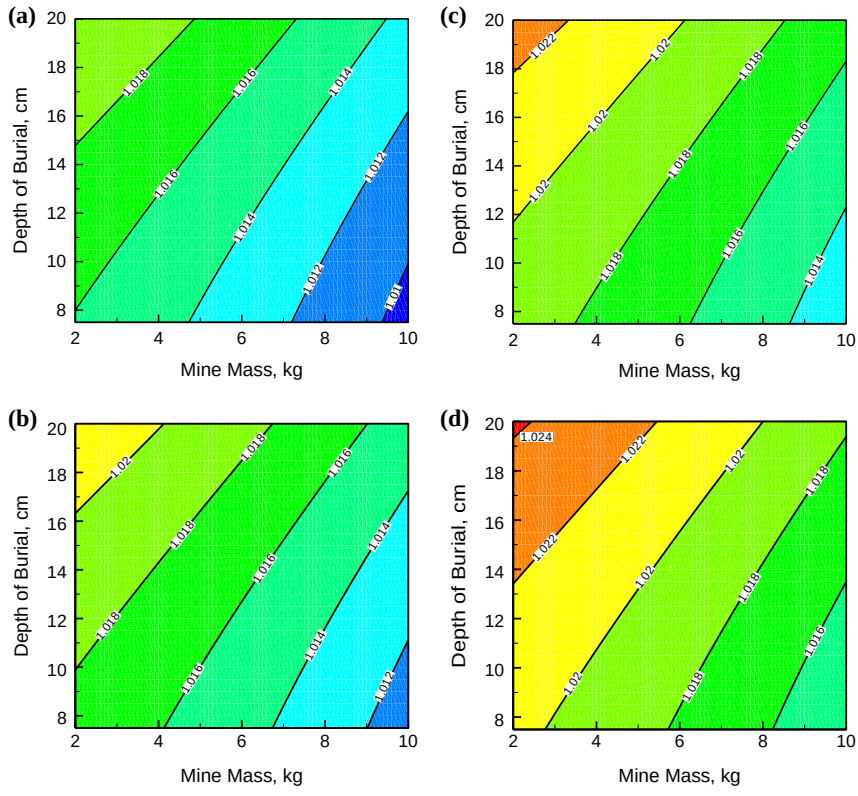

Notes: (a) 40 cm; (b) 60 cm; (c) 80 cm; (d) 100 cm

Figure 9.
The effect of landmine-mass and depth of burial on the ratio of the maximum accelerations of the top surface of the hull-floor made of composite-material and AISI 4340 steel, at four stand-off distances

identical to their counterparts used in Figures 7(a)-(d) and 8(a)-(d). As far as the contour lines are concerned, they correspond to the ratios of the maximum acceleration of the hull-floor top surface for the composite-material and steel cases. Examination of the results displayed in Figure 9(a)-(d) reveals that the maximum-acceleration ratio is greater than, but very close to, 1.0. The overall range of this quantity is approximately 1.010-1.024. In other words, the maximum acceleration associated with the steel-with-composite material replacement is expected to result in a 1.0-2.4 percent increase in the maximum acceleration of the hull-floor. This finding is consistent with the fact that, despite the composite hull-floor weighing between 52 and 64 percent of the steel hull-floor, the overall contribution of the hull-floor to the vehicle mass is only ca. 2.8-3.6 percent. Based on the findings displayed in Figure 9(a)-(d), it appears that the increase in the hull-floor maximum acceleration due to steel-to-composite material substitution is not excessive and, hence, would not act as a firm constraint on the considered material substitution.

3.4 Maximum deflection consideration

In the cases when the hull-floor has not ruptured, the maximum upward deflection of the hull-floor can also become important since, if excessive, it can severely compromise the available cabin space. In Figure 10(a)-(d), a series of contour plots corresponding to

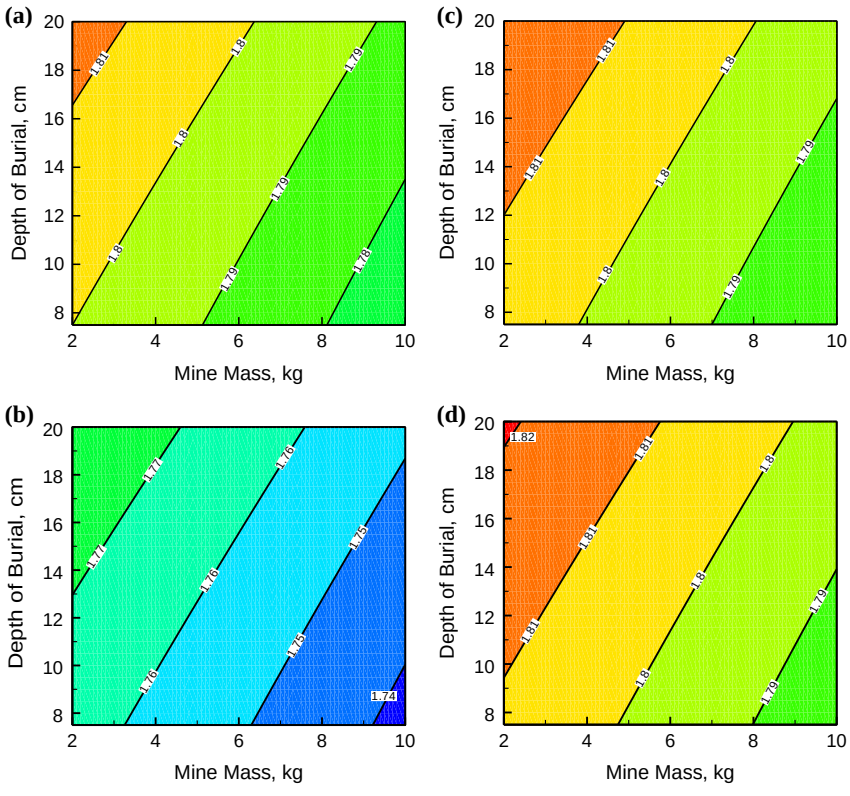

Notes: (a) 40 cm; (b) 60 cm; (c) 80 cm; (d) 100 cm

Figure 10.
The effect of landmine-mass and depth of burial on the ratio of the maximum upward deflections of the top surface of the hull-floor made of composite-material and AISI 4340 steel, at four stand-off distances

the ratio of the maximum upward deflections in the composite-material and steel hull-floor cases are given. Examination of the results displayed in Figure 10(a)-(d) reveals that this ratio is in the 1.74-1.82 range. In other words, the maximum (upward) deflection of the composite-material hull-floor is higher by 74-82 percent relative to that of the steel hull-floor. This increase in the hull-floor upward deflection can become a material-substitution limiting factor, particularly in the landmine-detonation cases associated with an optimal combination of the large explosive mass and the intermediate DOB (the conditions which lead to maximum transfer of the detonation-generated momentum to the target).

3.5 Spall total-momentum consideration

Another potential threat to the vehicle occupants arises from the spall which are generated at the top surface of the hull-floor and propelled inward at high velocities. Since composite-materials generally possess significantly lower (tensile) strength in the through-the-thickness direction relative to their in-plane strength, the increased threat of spallation accompanying steel-with-composite material substitution must be addressed. This was done in the present work by determining the total momentum of all the hull-floor finite-elements which were either detached from the rest of the floor-plate or had to be removed from the simulation due to their excessive distortion. The results of this procedure are depicted in Figure 11(a)-(d). The contour lines in these

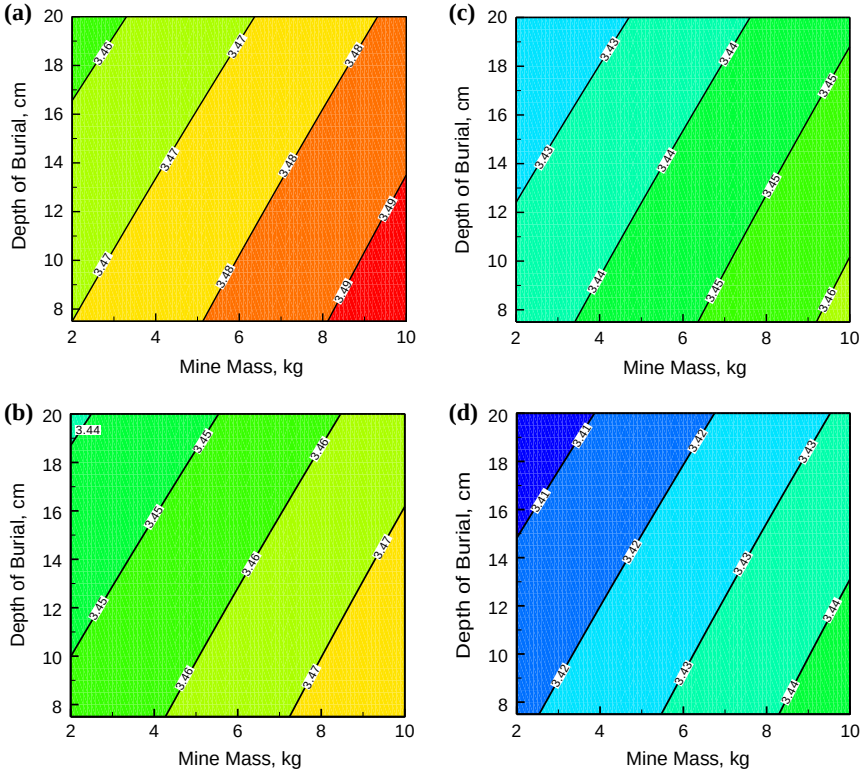

Notes: (a) 40 cm; (b) 60 cm; (c) 80 cm; (d) 100 cm

Figure 11.
The effect of landmine-mass and depth of burial on the ratio of the total momentum of all the spall fragments of the hull-floor made of the composite-material and AISI 4340 steel, at four stand-off distances

figures correspond to the ratio of the total momentum residing in these elements in the case of the composite-material and the steel hull-floors.

Examination of the results displayed in Figure 11(a)-(d) reveals that, in the case of the composite-material hull-floor, the total momentum carried by the spalled fragments is approximately 245 percent larger than that in the case of steel hull-floor. While this may appear to present a major constraint to the considered material substitution, it should be noted that the top surface of the composite-material hull-floor can be coated with a "spall-catching" material (e.g. a phenolic polymer layer) which could quite effectively alleviate the problem of excessive spallation of the composite hull-floor.

3.6 Effect of soil saturation

All the results presented and discussed so far were obtained for the case of dry soil. It is well-established (Grujicic *et al.*, 2008a) that soil saturation can significantly increase the extent of detonation-induced momentum transferred to the hull-floor. A comprehensive examination of the effect of soil-saturation on the potential ramifications of the steel-with-composite material substitution in hull-floors is beyond the scope of the present work. Nevertheless, the results of a few studies carried out for the case of fully saturated soil are shown in Figure 12(a)-(e). In these figures, the SOD was kept constant at 40 cm, while the contours were defined as the following quantities: ratio of the critical areal-densities of the composite-material and the steel; ratio of the critical thicknesses of the two hull-floor cases; ratio of the maximum acceleration of the two hull-floor top surfaces; ratio of the maximum upward deflections in the two hull-floor cases; and ratio of the total momentum residing in spall fragments for the two hull-floor cases. A comparison of the results displayed in Figure 12(a)-(e) with their counterparts shown in Figures 7(a), 8(a), 9(a), 10(a) and 11(a) reveals that, while the absolute values of the contour quantities is somewhat affected by the extent of soil saturation, the general findings regarding the potential ramifications of the steel hull-floors with their composite-material counterparts remain unchanged.

3.7 Final remarks

The results obtained in the present work clearly demonstrated the potential benefits resulting from the steel substitution with composite-material in military-vehicle hull-floors. These benefits are the result of the higher blast-protection mass-efficiency of the considered composite material with respect to its steel counterpart. Furthermore, the work presented also indicated some of the potential drawbacks associated with this material substitution, mainly relative to: decreases in the ground-clearance/cabin-space, due to the increase in the composite-material hull-floor thickness; decrease in the cabin-space, due to the increased upward deflection of the composite-material hull-floor; and increased extent of spallation from the top face of the hull-floor, due to the inferior through-the-thickness strength of the composite material analyzed. Consequently, the advantages and shortcomings associated with the considered material substitution must be properly weighted in each hull-floor design case, associated with the specific functional requirements relative to the hull-floor survivability to a given level of threat.

4. Summary and conclusions

Based on the results obtained in the present work, the following main summary remarks and conclusions can be drawn:

(1) The benefits and limitations accompanying potential substitution of steel with the fiber-reinforced polymer-matrix composite material in military-vehicle

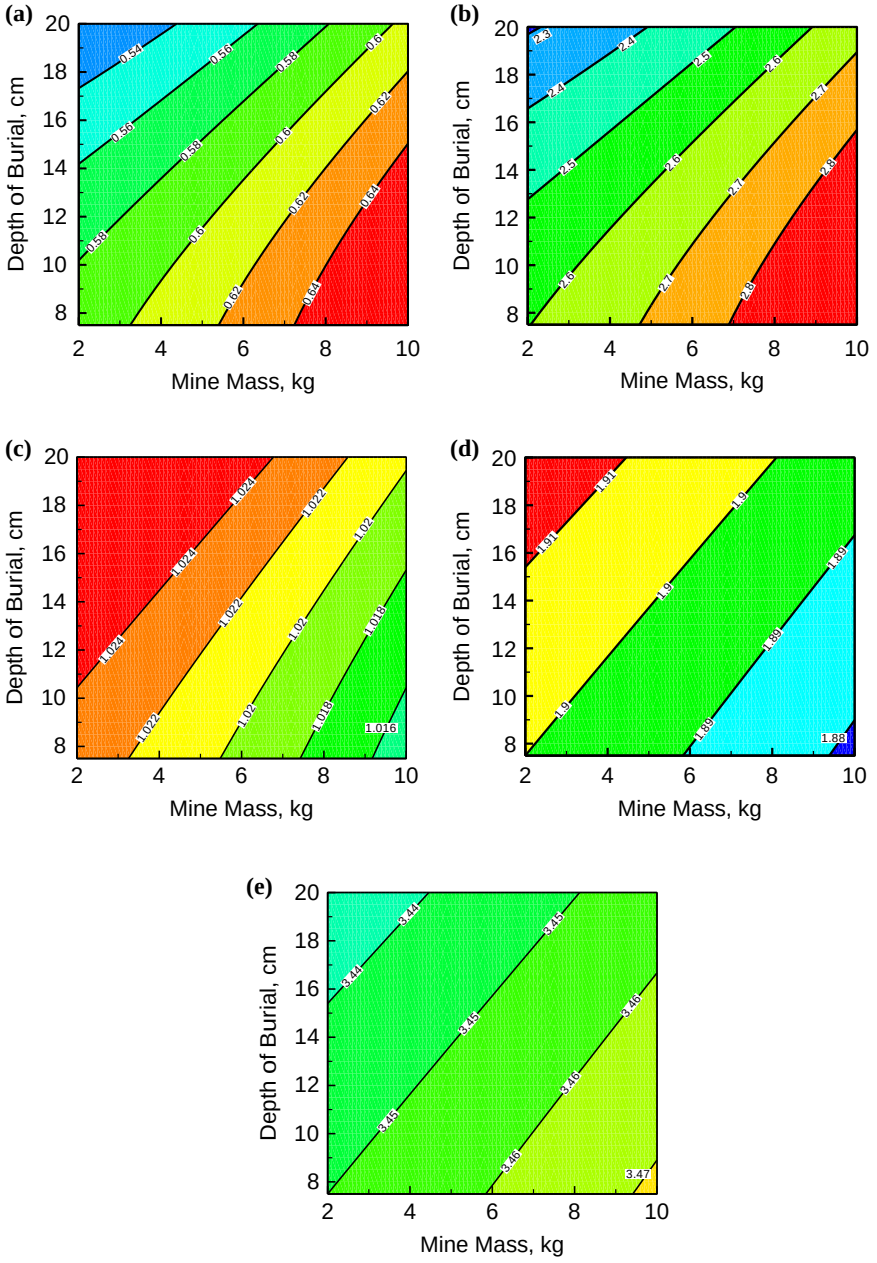

Notes: (a) "critical" mass efficiencies; (b) "critical" thicknesses; (c) maximum accelerations of the hull-floor top surface; (d) maximum upward deflections of the hull-floor top surface; (e) total momentum of all the spall fragments of the hull-floor

Figure 12.
The effect of landmine-mass and depth of burial, at a stand-off distance of 40 cm, in the case of saturated-soil, on the ratios

hull-floors is investigated using advanced coupled finite-element/discrete-particle computational methods and tools. The benefits and limitations are assessed relative to the primary function of the hull-floor to protect the vehicle occupants in the case of the underbelly buried landmine detonation.

(2) In the computational analysis, a large number of mine-detonation scenarios are investigated under physically realistic ranges of the landmine mass, its DOB in the soil, and the soil-surface/floor-plate distances.

(3) When identifying/quantifying the potential benefits/shortcomings associated with the considered material substitution, various threats to the vehicle occupants are considered, such as: hull-floor rupture; excessive upward acceleration of the hull-floor; excessive upward deflection of the hull-floor; and (iv) excessive spallation and release of high-velocity fragments from the top surface of the hull-floor.

(4) The results obtained clearly revealed both the benefits and the shortcomings associated with the examined material substitution, suggesting that they should be properly weighted in each specific case of hull-floor design, associated with the specific functional requirements relative to the hull-floor survivability to a given level of threat.

References

Baibuz, V.F., Zitserman, V.Y., Golubushkin, L.M. and Malyshev, I.G. (1986), "The co-volume and equation of state of high-temperature real gases", *Journal of Engineering Physics and Thermo-Physics*, Vol. 51 No. 2, pp. 955-956.

Bergeron, D., Hlady, S. and Braid, M.P. (2002), "Pendulum techniques to measure land mine blast loading", paper presented at the Seventh International MABS Symposium, Las Vegas, NV, June 10-14.

Bernoulli, D. (1738), *Hydrodynamica Sive de Viribus et Motibus Fluidorum Commentarii*, Johannis Reinholdi Dulseckeri, Argentorati, Strasbourg.

Bernoulli, D. and Bernoulli, J. (1968), *Hydrodynamics*, Dover Publications, Mineola, NY.

Børvik, T., Hanssen, A.G., Langseth, M. and Olovsson, L. (2009), "Response of structures to planar blast loads – a finite element engineering approach", *Computers and Structures*, Vol. 87 Nos 9/10, pp. 507-520.

Børvik, T., Olovsson, L., Hanssen, A.G., Dharmasena, K.P., Hansson, H. and Wadley, H.N.G. (2011), "A discrete particle approach to simulate the combined effect of blast and sand impact loading of steel plates", *Journal of the Mechanics and Physics of Solids*, Vol. 59 No. 5, pp. 940-958.

Braid, M.P. (2001), *Experimental Investigation and Analysis of the Effects of Anti-Personnel Landmine Blasts*, Suffield Special Publication, DRES SSSP 2001-188, Defence R&D Canada, Kingston, ON.

Clausius, R. (1880), "Ueber das verhalten der kohlensaüre in bezug auf druck, volume und temperature", *Annalen der Physik und Chemie*, Vol. 245 No. 3, pp. 337-357.

Dassault Systèmes (2013), *ABAQUS Version 6.13, User Documentation*, Dassault Systèmes, Waltham, MA.

Deshpande, V.S., McMeeking, R.M., Wadley, H.N.G. and Evans, A.G. (2009), "Constitutive model for predicting dynamic interactions between soil Ejecta and structural panels", *Journal of Mechanics and Physics of Solids*, Vol. 57 No. 8, pp. 1139-1164.

Frutschy, K.J. and Clifton, R.J. (1998), "High-temperature pressure-shear plate impact experiments on OFHC copper", *Journal of the Mechanics and Physics of Solids*, Vol. 46 No. 10, pp. 1723-1743.

Grujicic, M., Pandurangan, B., Huang, Y., Cheeseman, B.A., Roy, W.N. and Skaggs, R.R. (2007a), "Impulse loading resulting from shallow buried explosives in water-saturated sand", *Journal of Materials: Design and Applications*, Vol. 221 No. 1, pp. 21-35.

Grujicic, M., Pandurangan, B., Zecevic, U., Koudela, K.L. and Cheeseman, B.A. (2007b), "Ballistic performance of alumina/S-2 glass-reinforced polymer-matrix composite hybrid lightweight armor against armor piercing (AP) and Non-AP projectiles", *Multidiscipline Modeling in Materials and Structures*, Vol. 3 No. 3, pp. 287-312.

Grujicic, M., Pandurangan, B., Haque, I., Cheeseman, B.A. and Skaggs, R.R. (2007c), "A computational analysis of mine blast survivability of a commercial vehicle structure", *Multidiscipline Modeling in Materials and Structures*, Vol. 3 No. 4, pp. 431-460.

Grujicic, M., Pandurangan, B., Qiao, R., Cheeseman, B.A., Roy, W.N., Skaggs, R.R. and Gupta, R. (2008a), "Parameterization of the porous-material model for sand with different levels of water saturation", *Soil Dynamics and Earthquake Engineering*, Vol. 28 No. 1, pp. 20-35.

Grujicic, M., Pandurangan, B., Coutris, N., Cheeseman, B.A., Roy, W.N. and Skaggs, R.R. (2008b), "Computer-simulations based development of a high strain-rate, large-deformation, high-pressure material model for STANAG 4569 sandy gravel", *Soil Dynamics and Earthquake Engineering*, Vol. 28 No. 12, pp. 1045-1062.

Grujicic, M., Arakere, G., Nallagatla, H.K., Bell, W.C. and Haque, I. (2009a), "Computational investigation of blast survivability and off-road performance of an up-armored high-mobility multi-purpose wheeled vehicle (HMMWV)", *Journal of Automobile Engineering*, Vol. 223 No. 3, pp. 301-325.

Grujicic, M., Arakere, G., Bell, W.C. and Haque, I. (2009b), "Computational investigation of the effect of up-armoring on occupant injury/fatality reduction of a prototypical high-mobility multi-purpose wheeled vehicle subjected to mine-blast", *Journal of Automobile Engineering*, Vol. 223 No. 7, pp. 903-920.

Grujicic, M., Bell, W.C., Arakere, G. and Haque, I. (2009c), "Finite element analysis of the effect of up-armoring on the off-road braking and sharp-turn performance of a high-mobility multi-purpose wheeled vehicle (HMMWV)", *Journal of Automobile Engineering*, Vol. 223 No. 11, pp. 1419-1434.

Grujicic, M., Arakere, G., He, T., Bell, W.C., Glomski, P.S. and Cheeseman, B.A. (2009d), "Multi-scale ballistic material modeling of cross-plied compliant composites", *Composites Part B: Engineering*, Vol. 40 No. 6, pp. 468-482.

Grujicic, M., He, T., Pandurangan, B., Bell, W.C., Coutris, N., Cheeseman, B.A., Roy, W.N. and Skaggs, R.R. (2009e), "Development, parameterization and validation of a visco-plastic material model for sand with different levels of water saturation", *Journal of Materials: Design and Applications*, Vol. 223 No. 2, pp. 63-81.

Grujicic, M., Marvi, H., Arakere, G., Bell, W.C. and Haque, I. (2010a), "The effect of up-armoring the high-mobility multi-purpose wheeled vehicle (HMMWV) on the off-road vehicle performance", *Multidiscipline Modeling in Materials and Structures*, Vol. 6 No. 2, pp. 229-256.

Grujicic, M., Pandurangan, B., Coutris, N., Cheeseman, B.A., Roy, W.N. and Skaggs, R.R. (2010b), "Derivation, parameterization and validation of a sandy-clay material model for use in landmine detonation computational analyses", *Journal of Materials Engineering and Performance*, Vol. 19 No. 3, pp. 434-450.

Grujicic, M., Pandurangan, B. and Hariharan, A. (2011a), "Comparative discrete-particle vs continuum-based computational investigation of soil response to impulse loading", *Journal of Materials Engineering and Performance*, Vol. 20 No. 9, pp. 1520-1535.

Grujicic, M. and Bell, W.C. (2011b), "A computational analysis of survivability of a pick-up truck subjected to mine detonation loads", *Multidiscipline Modeling in Materials and Structures*, Vol. 7 No. 4, pp. 386-423.

Grujicic, M., Bell, W.C., Pandurangan, B., Yen, C.-F. and Cheeseman, B.A. (2011c), "Computational investigation of structured shocks in Al/SiC-particulate metal matrix composites", *Multidiscipline Modeling in Materials and Structures*, Vol. 7 No. 4, pp. 469-497.

Grujicic, M., Pandurangan, B., Bell, W.C., Yen, C.-F. and Cheeseman, B.A. (2011d), "Application of a dynamic-mixture shock-wave model to the metal-matrix composite materials", *Materials Science and Engineering A*, Vol. 528 No. 28, pp. 8187-8197.

Grujicic, M., Pandurangan, B., Yen, C.-F. and Cheeseman, B.A. (2012), "Modifications in the AA5083 Johnson-cook material model for use in friction stir welding computational analyses", *Journal of Materials Engineering and Performance*, Vol. 21 No. 11, pp. 2207-2217.

Grujicic, M., Pandurangan, B., Snipes, J.S., Yen, C.-F. and Cheeseman, B.A. (2013a), "Multi-length scale enriched continuum-level material model for Kevlar®-fiber reinforced polymer-matrix composites", *Journal of Materials Engineering and Performance*, Vol. 22 No. 3, pp. 681-695.

Grujicic, M., Yavari, R., Snipes, J.S. and Ramaswami, S. (2013b), "Extension of a current continuum-level material model for soil into the low-density discrete-particle regime", *Journal of Materials Engineering and Performance*, Vol. 22 No. 5, pp. 1268-1283.

Grujicic, M., Galgalikar, R., Snipes, J.S., Yavari, R. and Ramaswami, S. (2013c), "Multi-physics modeling of the fabrication and dynamic performance of all-metal auxetic-hexagonal sandwich-structures", *Materials and Design*, Vol. 51, pp. 113-130.

Holsapple, K.A. and Housen, K.R. (2004), "Crater database and scaling tools", available at: http://keith.aa.washington.edu/craterdata (accessed January 3, 2014).

Johnson, G.R. and Cook, W.H. (1983), "A constitutive model and data for metals subjected to large strains, high strain rates and high temperatures", *Proceedings of the Seventh International Symposium on Ballistics, The Hague*, April 19-21, pp. 541-547.

(The) Math Works Inc. (2013), *MATLAB Version 8.1.0.604, R2013*, The Math Works Inc., Natick, MA.

Maxwell, J.C. (1860), "Illustrations of the dynamical theory of gases", *Philosophical Magazine*, Vol. 19 No. 124, pp. 19-32.

Morris, B.L. (1993), "Analysis of improved crew survivability in light vehicles subjected to mine blast", Final Report for Contract No. DAAK70-92-C-0058 for the US Army Belvoir RDEC, Ft Belvoir, VA.

Olovsson, L., Hanssen, A.G. and Børvik, T. (2010), "A particle-based approach to close-range blast loading", *European Journal of Mechanics A/Solids*, Vol. 29 No. 1, pp. 1-6.

Puck, A. and Schurmann, H. (1998), "Failure analysis of FRP laminates by means of physical based phenomenological models", *Composite Science and Technology*, Vol. 58 No. 7, pp. 1001-1010.

Souers, P.C. (2007), "Cylinder test on C-4", Report UCRL-TR-230845, Energetic Materials Center, Lawrence Livermore National Laboratory, Livermore, CA, available at: https://e-reports-ext.llnl.gov/pdf/347222.pdf (accessed January 3, 2014).

Souers, P.C., Wu, B. and Haselman, L.C. Jr (1996), "Detonation equation of state at LLNL, 1995", Report UCRL-ID119262 Rev 3, Energetic Materials Center, Lawrence Livermore National Laboratory, Livermore, CA.

Westine, P.S., Morris, B.L., Cox, P.A. and Polch, E. (1985), "Development of computer program for floor plate response from land mine explosions", Contract Report No. 1345, US Army TACOM Research and Development Center, Warren, MI.

Yen, C.-F. (2012), "A ballistic material model for continuous-fiber reinforced composites", *International Journal of Impact Engineering*, Vol. 46, pp. 11-22.

Appendix 1

Overview of the Composite Material Model (Yen, 2012; Grujicic et al., 2013a)

In this section, a brief overview is provided of the rate-dependent composite-material model used in the present work. Since details of this model can be found in Yen (2012) and Grujicic *et al.* (2013a), the model will be reviewed only briefly and conceptually in the remainder of this section. The defining features of the model can be summarized as follows:

(1) the model is aimed at providing an accurate account of the three-dimensional nature of the stress/strain states, high strain rates and high pressures encountered during ballistic-/blast-impact of composite laminates reinforced with plain-woven fabric;

(2) the material model is strain-based and utilizes the concept of a ply-/lamina-averaged local strain;

(3) the model incorporates Mohr-Coulomb (Puck and Schurmann, 1998) shear strength effects, i.e. it accounts for the fact that the (matrix) in-plane shear strength is generally a function of the (tensile/compressive) character and magnitude of the through-the-thickness lamina strain;

(4) the model accounts for the following fiber-reinforcement and matrix failure modes: (i) fiber failure due to a combination of axial tensile and transverse shear strains; (ii) fiber buckling failure due to axial compressive strains; (iii) fiber crushing failure due to lamina through-the-thickness compressive strains; (iv) matrix in-plane shear failure; and (v) matrix delamination failure due to a combined effect of the through-the-thickness tensile strains and transverse shear strains. It should be noted that since within the damage modes (i) and (ii), a distinction is made between the warp and weft fibers, the effective number of failure modes is seven rather than five; and

(5) the model is essentially of a linear-elastic orthotropic type with progressively degradable elastic stiffness constants. In other words, a generalized Hooke's law relation is assumed to hold between stress and strain quantities while damage is treated as a process which takes place gradually during ballistic-/blast-impact. Consequently, the model relies on the definition of the damage initiation criteria and the corresponding damage evolution laws.

A.1 Damage initiation criteria

In this subsection, a brief overview is provided of the basic concepts used to construct the functional relations (not repeated here since they could be found in Yen, 2012; Grujicic *et al.*, 2013a) defining the onset (and continuation) of damage for each of the five aforementioned fiber/matrix failure modes.

Fiber damage under combined axial-tension and transverse-shear: The onset and progression of this failure mode is assumed to be defined by a superposition of the quadratic contributions of the axial tensile and transverse shear strains. Furthermore, the laminate transverse shear strength is assumed to be controlled by the corresponding shear strength of the fiber itself and separate parameterizations are used for the warp and weft fibers.

Fiber damage under axial-compression: The onset and progression of this failure mode is assumed to be defined by the compressive axial strains whose effect is modulated by the lamina through-the-thickness compressive strain. In other words, axial-compression-induced fiber buckling is resisted by the stabilizing effect of the through-thickness compressive strain. Again, separate parameterizations are used for the warp and weft fibers.

Fiber damage under transverse compressive loading: This failure mode involves (both warp and weft) fiber crushing under sufficiently high through-the-thickness compressive strain.

Matrix in-plane shear failure: This mode of failure is associated with the fact that the matrix shear strength is lower than the fiber shear strength and that the composite material in question

possesses a laminated architecture. Consequently, sufficiently high in-plane shear strains may cause matrix shear failure without giving rise to any significant fiber damage.

Matrix delamination due to through-the-thickness tensile and shear stresses: This mode of failure also gives rise to the matrix in-plane failure. The effect of through-the-thickness compressive normal strains on the matrix shear-strength is accounted for through the use of the Mohr-Coulomb law. Furthermore, the effect of stress concentration in the region surrounding the boundary of the partially delaminated matrix is also accounted for in the model.

A.2 Damage evolution and material degradation

Key concepts associated with the construction of the material damage evolution laws and the accompanying material degradation functional relations are overviewed in this subsection.

Damage surface: Functional relations associated with the five-mode damage initiation define, within the strain-space, a damage initiation surface. As the composite-material degrades, the failure surface expands (i.e. additional straining is required to produce additional damage). Within the present composite-material model, damage progression is assumed to cause degradation in material stiffness, but not in the material strength properties.

Stiffness degradation variables: To account for the aforementioned damage-induced material-stiffness degradation, stiffness-degradation variables (one for each independent elastic constant/modulus), are first introduced. Then, each of the instantaneous (degraded) material-stiffness constants is obtained by multiplying its original/undegraded value by the instantaneous value of the corresponding damage variable. The instantaneous values of the damage variables are obtained through time integration of the corresponding degradation-variable evolution equation (defined by the model).

Damage evolution laws: For each of the five damage modes, the appropriate damage-evolution equation is defined as a function of all local-strain components. These equations are defined under the conditions that: the progression of damage of a given type occurs only if the additional loading places the strain outside the corresponding damage surface; and both the material damage and the associated stiffness-property degradation are irreversible.

Derivation of the damage/stiffness-coupling matrix: Next, the damage/stiffness coupling matrix is defined to quantify the sensitivity of different elastic-stiffness moduli to the extent of damage of different modes. Toward that end, the following assumptions are made:

(1) damage of the weft and warp fibers both in tension and transverse shear and in compression degrades the associated Young's modulus and shear moduli;

(2) fiber-crushing damage mode degrades all elastic moduli;

(3) in the case of the in-plane shear failure, only the associated shear modulus is affected; and

(4) delamination degrades the through-the-thickness Young's modulus as well as the two transverse shear moduli.

Integrated form of the stiffness degradation variables: By combining the evolution equations for the stiffness-degradation variables, the evolution equations for different damage modes, the damage/stiffness coupling matrix, and through proper time-integration, the contribution of each of the five damage modes to the instantaneous value of each of the stiffness degradation variables is obtained.

Residual stiffness: At sufficiently high levels of material damage, some of the stiffness-moduli can degrade to a zero value. This condition corresponds to a complete loss of the material load-bearing capacity relative to the diminished elastic modulus. But although this scenario is physically realistic for some of the damage/failure modes, e.g. the fiber failure under axial tension/transverse shear, it may not be fully realistic under other failure modes, e.g. fiber axial compression. Consequently, the governing equations of the model have been revised to include the nonzero residual elastic moduli under the following damage modes: fiber axial compression; and in the case of delamination in the presence of compressive strains.

A.3 Rate-dependency of stiffness and strength

Within the model, strain-rate dependence of both the stiffness and strength (one quantity per each damage mode) properties are accounted for through the use of the appropriate scaling functional relations.

A.4 Material model parameterization

The original model presented by Yen (2012) contained 24 parameters: 14 strength parameters; six stiffness parameters; two rate dependency parameters; and two damage parameters. These parameters are commonly assessed by applying regression analysis to the results from a variety of mechanical tests over a range of strain rates. The large number of the model parameters makes this parameterization effort quite cumbersome, time-consuming and costly. In addition, the model extension presented by Grujicic *et al.* (2013a) added a stochastic character to some of the model parameters, requiring the definition of the appropriate probability distribution functions for these parameters. These distribution functions extended the list of the parameters, making model parameterization even costlier. To overcome this challenge, a multi-length scale computational approach was introduced by Grujicic *et al.* (2013a) which enabled establishment of the appropriate distribution functions through the use of time-efficient, low-cost computational methods and tools.

Complete parameterization of the present composite-material model can be found in Grujicic *et al.* (2013a).

Appendix 2

Extended Johnson-Cook material model (Grujicic et al., 2012)

Within the generalized Johnson-Cook material model, the hydrostatic and deviatoric constitutive behavior of a (metallic) material are treated separately and ultimately combined.

Hydrostatic response

The hydrostatic portion of the stress is handled using the EOS which relates pressure to the material mass-density and the internal-energy-density/temperature. For high-strength steels like AISI 4340, a linear-elastic EOS is generally considered as an appropriate choice.

Deviatoric response

The deviatoric portion of the stress in the elastic region is handled using the generalized Hooke's Law. As far as the deviatoric plastic response of the material is concerned, it is represented by combining: a von-Mises type of the yield criterion; a normality flow rule; and a classical Johnson-Cook yield-strength relationship (Johnson and Cook, 1983). The Johnson-Cook strength model enables representing the material behavior displayed under large-strain, high deformation rate, high-temperature conditions, of the type encountered in problems dealing with hypervelocity impact and penetration conditions.

Damage/failure model

To model the progressive evolution of damage and ultimate failure, the classical Johnson-Cook failure model (Grujicic *et al.*, 2007b) is used. Within this model, damage is incremented within the given loading step by the amount equal to the ratio of the equivalent plastic-strain increment and the (mean-stress-, effective-stress-, strain-rate- and homologous-temperature-dependent) failure-strain.

Material-model parameterization

All generalized Johnson-Cook material mode parameters for AISI 4340 steel can be found in Grujicic *et al.* (2013c).

About the authors

M. Grujicic, is a Professor in the Department of Mechanical Engineering at the Clemson University. M. Grujicic's research interests include computational engineering. Professor M. Grujicic is the corresponding author and can be contacted at: gmica@clemson.edu

Dr J.S. Snipes is a Post-Doctoral Fellow in the Department of Mechanical Engineering at the Clemson University. Dr J.S. Snipes's research interests include computational material modeling.

Dr S. Ramaswami is a Post-Doctoral Fellow in the Department of Mechanical Engineering at the Clemson University. Dr S. Ramaswami's research interests include computational material modeling.

R. Yavari is a Graduate Student in the Department of Mechanical Engineering at the Clemson University. R. Yavari's research interests include multi-physics modeling of various materials phenomena and processes.

Dr C.-F. Yen is a Research Engineer at the Army Research Labs, Aberdeen Proving Ground. Dr C.-F. Yen's research interests include composite modeling.

Dr B.A. Cheeseman is a Research Engineer at the Research Labs, Aberdeen Proving Ground. Dr B.A. Cheeseman's research interests include blast modeling and simulation.